University of Nebraska - Lincoln

DigitalCommons@University of Nebraska - Lincoln

Faculty Publications from the Center for Plant Science Innovation

Plant Science Innovation, Center for

2014

Methylation protects microRNAs from an AGO1-associated activity that uridylates 5′ RNA fragments generated by AGO1 cleavage

Guodong Ren
University of Nebraska-Lincoln, gren2@unl.edu

Meng Xie
University of Nebraska–Lincoln

Shuxin Zhang
University of Nebraska-Lincoln, szhang2@unl.edu

Carissa Vinovskis
University of Nebraska–Lincoln

Xuemei Chen
University of California - Riverside, xuemei.chen@ucr.edu

See next page for additional authors

Follow this and additional works at: http://digitalcommons.unl.edu/plantscifacpub

Part of the Plant Biology Commons, Plant Breeding and Genetics Commons, and the Plant Pathology Commons

Authors

Guodong Ren, Meng Xie, Shuxin Zhang, Carissa Vinovskis, Xuemei Chen, and Bin Yu

Methylation protects microRNAs from an AGO1-associated activity that uridylates 5′ RNA fragments generated by AGO1 cleavage

Guodong Ren[a,b,1], Meng Xie[a,1], Shuxin Zhang[a], Carissa Vinovskis[a], Xuemei Chen[c,d,2], and Bin Yu[a,2]

[a]Center for Plant Science Innovation and School of Biological Sciences, University of Nebraska–Lincoln, Lincoln, NE 68588-0660; [b]State Key Laboratory of Genetic Engineering, Department of Biochemistry and Institute of Plant Biology, School of Life Sciences, Fudan University, Shanghai 200433, China; and [c]Department of Botany and Plant Sciences and Institute of Integrative Genome Biology and [d]Howard Hughes Medical Institute, University of California, Riverside, CA 92521

In plants, methylation catalyzed by HEN1 (small RNA methyl transferase) prevents microRNAs (miRNAs) from degradation triggered by uridylation. How methylation antagonizes uridylation of miRNAs in vivo is not well understood. In addition, 5′ RNA fragments (5′ fragments) produced by miRNA-mediated RNA cleavage can be uridylated in plants and animals. However, the biological significance of this modification is unknown, and enzymes uridylating 5′ fragments remain to be identified. Here, we report that in *Arabidopsis*, HEN1 suppressor 1 (HESO1, a miRNA nucleotidyl transferase) uridylates 5′ fragments to trigger their degradation. We also show that Argonaute 1 (AGO1), the effector protein of miRNAs, interacts with HESO1 through its Piwi/Argonaute/Zwille and PIWI domains, which bind the 3′ end of miRNA and cleave the target mRNAs, respectively. Furthermore, HESO1 is able to uridylate AGO1-bound miRNAs in vitro. miRNA uridylation in vivo requires a functional AGO1 in *hen1*, in which miRNA methylation is impaired, demonstrating that HESO1 can recognize its substrates in the AGO1 complex. On the basis of these results, we propose that methylation is required to protect miRNAs from AGO1-associated HESO1 activity that normally uridylates 5′ fragments.

Small interfering RNAs (siRNAs) and microRNAs (miRNAs), ~20–25 nucleotides (nt) in size, are important regulators of gene expression. miRNAs and siRNAs are derived from imperfect hairpin transcripts and perfect long double-stranded RNAs, respectively (1, 2). miRNAs and siRNAs are then associated with Argonaute (AGO) proteins to repress gene expression through target cleavage and/or translational inhibition (3). The cleavage of target mRNAs usually occurs at a position opposite the tenth and eleventh nucleotides of miRNAs, resulting in a 5′ RNA fragment (5′ fragment) and a 3′ fragment (4). In *Arabidopsis*, the major effector protein for miRNA-mediated gene silencing is AGO1, which possesses the endonuclease activity required for target cleavage (5–7). In *Drosophila*, the exosome removes the 5′ fragments through its 3′-to-5′ exoribonuclease activity (8). How 5′ fragments are degraded in higher plants remains unknown. It has been shown that the 5′ fragments are subject to untemplated uridine addition at their 3′ termini (uridylation) in both animals and plants (9). However, the biological significance of this modification remains unknown because of a lack of knowledge of the enzymes targeting 5′ fragments for uridylation.

Uridylation plays important roles in regulating miRNA biogenesis. In animals, TUT4, a terminal uridyl transferase, is recruited by Lin-28 (an RNA binding protein) to the let-7 precursor (prelet-7), resulting in uridylation of prelet-7 (10, 11). This modification impairs the stability of prelet-7, resulting in reduced levels of let-7. In addition, monouridylation has been shown to be required for the processing of some miRNA precursors (12). Deep sequencing analysis reveals that precursor uridylation is a widespread phenomenon occurring in many miRNA families in animals (13). Uridylation also regulates the function and stability of mature miRNAs and siRNAs in both

animals and plants (14–16). Uridylation of miR26 in animals reduces its activity without affecting its stability (17). In contrast, uridylation of some siRNAs in *Caenorhabditis elegans* restricts them to CSR-1 (an AGO protein) and reduces their abundance, which is required for proper chromosome segregation (18). In the green algae *Chlamydomonas reinhardtii* and the flowering plant *Arabidopsis*, uridylation causes the degradation of miRNAs and siRNAs (19–21). Enzymes that uridylate miRNAs and siRNAs have been identified in both animals and plants. In humans and *C. elegans*, terminal uridyl transferases zinc finger, CCHC domain containing (ZCCHC) 6, ZCCHC11, terminal uridylyl transferase 1, and other enzymes have been shown to uridylate miRNAs in a miRNA sequence-specific manner (22), whereas HESO1 acts on most miRNAs and siRNAs in *Arabidopsis* (20, 21). Nevertheless, it is unclear how these terminal uridyl transferases recognize their targets.

Here we show that HESO1 catalyzes the uridylation of 5′ fragments produced by AGO1-mediated cleavage of miRNA target RNAs. Uridylation of the 5′ fragment of *MYB domain protein 33* (*MYB33-5′*; a target of miR159) is impaired in *heso1-2*, resulting in increased abundance of *MYB33-5′*. In addition, the proportion of *MYB33-5′* with 3′ truncation is increased in *heso1-2* compared with in wild-type plants. These results demonstrate that HESO1-mediated uridylation triggers 5′ fragment degradation through a mechanism that may be different from 3′-to-5′ trimming activity. Furthermore, we show that HESO1 interacts with AGO1 and is able to uridylate AGO1-bound miRNAs in vitro. On the basis of these observations, we propose that HESO1

GENETICS

Fig. 1. HESO1 uridylates 5′ fragments. (*A*) HESO1 uridylates a long single-stranded RNA (ssRNA) in vitro. A 5′-end [^{32}P]-labeled ssRNA was incubated with buffer, MBP, or MBP-HESO1 in the presence of UTP for 120 min, and products were resolved on a denaturing polyacrylamide gel. (*B*) Uridine addition (red rectangle) at the 3′ end of the cleavage site of *MYB33-5′*. ▲ and ▼ represent the adaptor. (*C*) Uridylation of 5′ fragments in L*er* and *heso1-2*. Uridines in lowercase indicate that they can alternatively be considered as a templated addition. The numbers of clones for each modification were shown in parentheses. Clones are the numbers of sequenced clones. Ratio is the frequency of clones with 3′-end modifications among sequenced clones.

can uridylate AGO1-associated 5′ fragments and miRNAs, resulting in their degradation.

Results

HESO1 Uridylates 5′ RNA Fragments Generated by miRNA-Mediated Cleavage. HESO1 possesses terminal uridyl transferase activity on 21-nt small RNAs in vitro (20, 21). However, whether HESO1 acts on other RNAs is not known. To address this question, we generated a [^{32}P]-labeled single-stranded RNA (ssRNA; ~100 nt), which corresponds to a portion of *UBQ5* mRNA through in vitro transcription. HESO1 lengthened this ssRNA in the presence of UTP (Fig. 1*A*). This result suggested that HESO1 might have substrates other than small RNAs and, therefore, prompted us to test whether 5′ fragments are also substrates of HESO1. We compared 5′ fragment uridylation in the null *heso1-2* mutant (20) with that in Landsberg *erecta* (L*er*; wild-type control of *heso1-2*), using a 3′ adaptor-ligation mediated rapid amplification of cDNA ends (al-RACE) approach. Total RNAs from L*er* or *heso1-2* were isolated, ligated to a 3′ adapter, and reverse-transcribed with a primer recognizing the 3′ adapter. Seminested PCR was subsequently performed to amplify 5′ fragments generated by AGO1 slicing of *MYB domain protein 33* (*MYB33-5′*), *Auxin Response Factor 10* (*ARF10-5′*), and *Lost Meristems 1* (*LOM1-5′*), which are targets of miR159, miR160, and miR171, respectively (23–26). PCR products of the expected sizes were

gel-purified, cloned, and sequenced (Fig. S1), and 75%, 59.1%, and 26.5% of *MYB33-5′*, *ARF10-5′*, and *LOM1-5′* were uridylated in L*er*, respectively (Fig. 1 *B* and *C* and Dataset S1). In contrast, the proportions of uridylated *MYB33-5′*, *ARF10-5′*, and *LOM1-5′* were reduced to 5.9%, 23.8%, and 12.9% in *heso1-2*, respectively (Fig. 1 *B* and *C* and Dataset S1). Furthermore, the 3′ tail length of 5′ fragments was reduced in *heso1-2* compared with

Fig. 2. HESO1-mediated uridylation triggers the degradation of *MYB33-5′*. (*A*) A schematic diagram of the *MYB33* cDNA showing the positions of probes used for Northern blotting analyses. The filled circle represents the stop codon. ▲ represents the cleavage site. (*B*) The abundance of *MYB33-5′* was higher in *heso1-2* than in L*er*. *MYB33* RNAs were detected by Northern blotting, using probes (shown in *A*) recognizing *MYB33-5′* or *MYB33-3′* generated by AGO1-mediated cleavage. FL, full-length *MYB33* transcripts; CP, cleavage product; *myb33*, a mutant allele of *MYB33* in which a T-DNA insertion disrupts the transcription of *MYB33* (26). The levels of cleavage products in *heso1-2* were normalized to FL transcripts and compared with those in L*er*. (*C*) Northern Blot analysis of miR159 in L*er* and *heso1-2*. U6 RNA was probed as a loading control. Note that the miR159 probe also recognizes miR319.

Fig. 3. cRACE analysis of *MYB33-5′*. (*A*) and (*B*) Schematic diagrams of cRACE followed by nested RT-PCR (cRT-PCR), used to analyze capped (black) or uncapped (gray) *MYB33-5′*. (*C*) A schematic diagram of the *MYB33* cDNA showing the positions of primers for nested RT-PCR. ▼ represents the cleavage site. (*D*) Analyses of 5′ and 3′ ends of *MYB33-*5′. The 3′-end signature (*y* axis) of individual *MYB33-5′* clones was plotted against its 5′-end position (*x* axis). The values on the *x* axis indicate the 5′ positions of individual *MYB33-5′* clones relative to the translation start site that is set as +1. The positive values on the *y* axis indicate the lengths (nt) of 3′ tailing while the negative values on the *y* axis represent the degree of 3′ truncation that is calculated as $-\mathrm{Log}_2(-N+1)$, where N represents the distance between the 3′-end position of *MYB33-5′* with 3′ truncation to the miRNA cleavage site, which is set as 0. The reason to use $\mathrm{Log}_2(-N+1)$ instead of $\mathrm{log}_2 N$ is to include clones with one nucleotide truncation on the plot. Different colors were used to distinguish clones with the same 5′-end signature: first, black; second, red; third, blue; fourth, cyan; fifth, pink. 5′ UTR, 5′ untranslated region; CDS, coding sequence. (*E*) The frequency of 3′-end uridylation in L*er* and *heso1-2*. (*F*) The proportions of 3′ truncated *MYB33-5′* in *heso1-2* and L*er*. The proportion indicates the frequency of 3′ truncated clones among all sequenced clones of cRT-PCR products. n, numbers of sequenced clones.

that in L*er* (1-3nt versus 1–15 nt; Fig. 1*C*). These results, together with the in vitro activity analysis (Fig. 1 *A* and *C*), demonstrated that HESO1 catalyzes uridylation of 5′ fragments generated by miRNA-mediated cleavage. However, the presence of uridylated 5′ fragments in the null *heso1-2* mutant (Fig. 1*C*) indicated that additional HESO1 homologs might also act on 5′ fragments.

HESO1-Mediated Uridylation Triggers the Degradation of the 5′ Fragment of *MYB33* Generated by AGO1 Cleavage. Next, we examined whether uridylation induced the degradation of 5′ fragments, using *MYB33* as a reporter RNA. *MYB33* was selected because the majority of its 5′ fragments (*MYB33-5′*) are uridylated (Fig. 1*C*) (9). We compared the accumulation of *MYB33-5′* in *heso1-2* with that in L*er* by Northern blotting, with probes recognizing *MYB33-5′* (Fig. 2*A*). To determine the specificity of probe for *MYB33-5′*, we included a *myb33* mutant in which a transfer (T)-DNA insertion abolished the transcription of *MYB33* (26). We were able to detect *MYB33-5′* in L*er* and *heso1-2*, but not in *myb33*. The levels of *MYB33-5′* increased in *heso1-2* relative to those in L*er* (Fig. 2*B*). This could be a result of the enhanced cleavage of *MYB33* by AGO1 or decreased degradation of *MYB33-5′*. If increased levels of *MYB33-5′* were caused by enhanced target cleavage, the abundance of *MYB33-3′* would increase as well. Our data showed that the levels of *MYB33-3′* were similar in *heso1-2* to those in L*er* (Fig. 2*B*), indicating that miRNA-mediated *MYB33* cleavage did not increase in *heso1-2*. Consistent with this observation, the levels of miR159 were not altered and the abundance of *MYB33* was only slightly elevated in *heso1-2* (Fig. 2 *B* and *C* and Fig. S2*A*). Thus, we concluded that HESO1-mediated uridylation promotes 5′ fragment degradation.

***heso1-2* Increases the Proportion of 3′ Truncated *MYB33-5′*.** Next we asked whether uridylation could trigger 3′-to-5′ degradation of *MYB33-5′*, as 5′ fragments can be degraded from the 3′ end by the exosome in *Drosophila* and in the green algae *C. reinhardtii*

(8, 27). The 3′ ends of both capped and uncapped *MYB33-5′* in L*er* and *heso1-2* were examined separately, as they both contain U-tails (9). We used a circularized rapid amplification of cDNA ends (cRACE; Fig. 3 *A–C*) approach to analyze the 3′ ends. Two ligation experiments were performed. In the first set of experiments, RNAs were self-ligated to analyze uncapped *MYB33-5′*, whose 5′ monophosphate allows self-ligation (Fig. 3*A*). In contrast, the self-ligation of capped *MYB33-5′* was blocked by the cap structure (Fig. 3*A*). In the second set of experiments, total RNAs were treated with alkaline phosphatase, calf intestinal (CIP), which removes the 5′ monophosphate and thus inhibits self-ligation of uncapped 5′ fragments (Fig. 3*B*). The resulting RNAs were further treated with tobacco acid pyrophosphatase (TAP) to remove the cap structure of capped RNAs, resulting in RNAs with a 5′ monophosphate. After this step, RNAs were ligated, which enabled us to analyze the capped 5′ fragments (Fig. 3*B*). Nested RT-PCR was then performed, using the ligation products generated from these two sets of experiments as templates (Fig. 3*C* and Fig. S2*B*). RT-PCR products were directly cloned and sequenced (Dataset S2). Both capped and uncapped *MYB33-5′* contained U-tails in L*er* (Fig. 3 *D* and *E*). However, the relative levels of uridylated *MYB33-5′* in the capped population were lower than those in the uncapped population in L*er* (Fig. 3 *D* and *E*). The relative levels of uridylated *MYB33-5′* in both capped and uncapped populations were reduced in *heso1-2* compared with L*er* (Fig. 3 *D* and *E*), consistent with our al-RACE results (Fig. 1*C*). We compared the levels of 3′ truncated *MYB33-5′* in *heso1-2* and L*er*. If uridylation triggered 3′-to-5′ degradation, lack of uridylation in *heso1-2* should reduce the proportion of 3′ truncated *MYB33-5′*. However, the proportion of both capped and uncapped 5′ fragments with 3′ truncation increased in *heso1-2* relative to L*er* (59.1% versus 47.1% for capped ones; 48% versus 19.1% for uncapped ones; Fig. 3*F*), suggesting that 3′ trimming of 5′ fragments may compete with uridylation. We also examined whether *heso1-2* had

any effect on the 5′-to-3′ truncation of uncapped *MYB33-5′*. However, no obvious changes for the positions of 5′ truncation were observed in *heso1-2* relative to Ler (Fig. 3D).

Exoribonuclease 4 Can Degrade 5′ Fragments. Studies have shown that exoribonucleases are involved in the degradation of RNA products generated by miRNA-mediated cleavage in *Drosophila* and *C. reinhardtii* (8, 27). We therefore asked whether exoribonucleases have roles in degrading 5′ fragments in *Arabidopsis*. We examined whether exoribonuclease 4 (XRN4), which is a major cytoplasmic 5′-to-3′ exoribonuclease in *Arabidopsis* (28, 29), could degrade *MYB33-5′*. The levels of *MYB33-5′* in *xrn4-5*, in which a T-DNA insertion completely abolished XRN4 function (29), were higher than those in wild-type control (Col) by Northern blotting. In contrast, the full-length *MYB33* transcript was not obviously affected by *xrn4-5* (Fig. S3), suggesting that the 5′ fragments are subjected to 5′-to-3′ degradation in *Arabidopsis*. We also tested the function of the exosome components CSL4 and RRP6L in *MYB33-5′* degradation. Northern blotting showed that the levels of *MYB33-5′* in *csl4-1* and *rrp6l1-1 rrp6l2-1 rrp6l3-1* were comparable with those in Col (Fig. S3), suggesting that CSL4 and RRP6L may not be involved in 5′ fragment degradation.

HESO1 Interacts with AGO1. Next we asked how HESO1 recognizes miRNAs and 5′ fragments. Because both miRNAs and 5′ fragments are associated with AGO1 during the cleavage process, we hypothesized that HESO1 might interact with AGO1 to recognize its substrates. Consistent with this hypothesis, AGO1 is associated with uridylated miRNAs (15, 30). We first examined whether HESO1 colocalized with AGO1. We coexpressed HESO1 fused with a red fluorescence protein (HESO1-RFP) and AGO1 fused with a yellow fluorescence protein (AGO1-YFP-HA) in *Nicotiana benthamiana*. The yellow fluorescence signal produced from AGO1-YFP overlapped with the red fluorescence signal generated by HESO1-RFP (Fig. 4A), indicating that HESO1 and AGO1 might be associated with each other.

To confirm the AGO1–HESO1 interaction, we performed reciprocal coimmunoprecipitation assays. We transiently expressed HESO1-YFP (20) in leaves of *N. benthamiana*, mixed the HESO1-YFP containing protein extracts with the AGO1 containing protein extracts from *Arabidopsis* inflorescence, and performed immunoprecipitation with either anti-AGO1 antibody (Fig. 4B and Fig. S4A) or anti-YFP antibody (Fig. 4C). We were able to detect HESO1-YFP (∼95 kDa) in the AGO1 immunoprecipitates and AGO1 (∼120 kDa) in the HESO1-YFP immunoprecipitates (Fig. 4 B and C). In contrast, YFP (∼26 kDa) and AGO1 did not coimmunoprecipitate (co-IP) with each other (Fig. 4 B and C). In addition, protein A beads without antibody failed to pull down either AGO1 or HESO1-YFP (Fig. 4 B and C). As both AGO1 and HESO1 recognize RNAs, it is possible that the AGO1-HESO1 interaction might be RNA-mediated. To test this, we treated the protein extracts with RNase A during the immunoprecipitation. We used this assay previously to show the RNA-dependent factor of DNA methylation 1-AGO4 interaction (31). This treatment did not abolish the AGO1-HESO1 interaction, suggesting that HESO1 may interact with AGO1 in an RNA-independent manner (Fig. S4B).

We next asked which domains of AGO1 interact with HESO1. We expressed five N-terminal 10XMYC-fused AGO1 fragments named FL (full-length; ∼150 kDa), A1 (aa 1–390; the N-terminal domain; ∼80 kDa), A2 [aa 381–530; the Piwi/Argonaute/Zwille (PAZ) domain; ∼40 KDa], A3 [aa 521–700; the linker2-middle (L2-Mid) domain; ∼45 kDa], and A4 (aa 671–1050; the PIWI domain; ∼75 kDa; Fig. 4D) individually in *N. benthamiana* and performed coimmunoprecipitation with HESO1-YFP. The PAZ and PIWI domains (A2 and A4), but not the N-terminal and L2-MID domains, interacted with HESO1 (Fig. 4E). We also identified the protein domains of HESO1 that mediate the AGO1–HESO1 interaction. Two fragments of HESO1 (Fig. 4F), an N-terminal fragment, which covers the poly(A) polymerase domain (PAP/25A) and the PAP-associated domain (aa 1–320; T1;
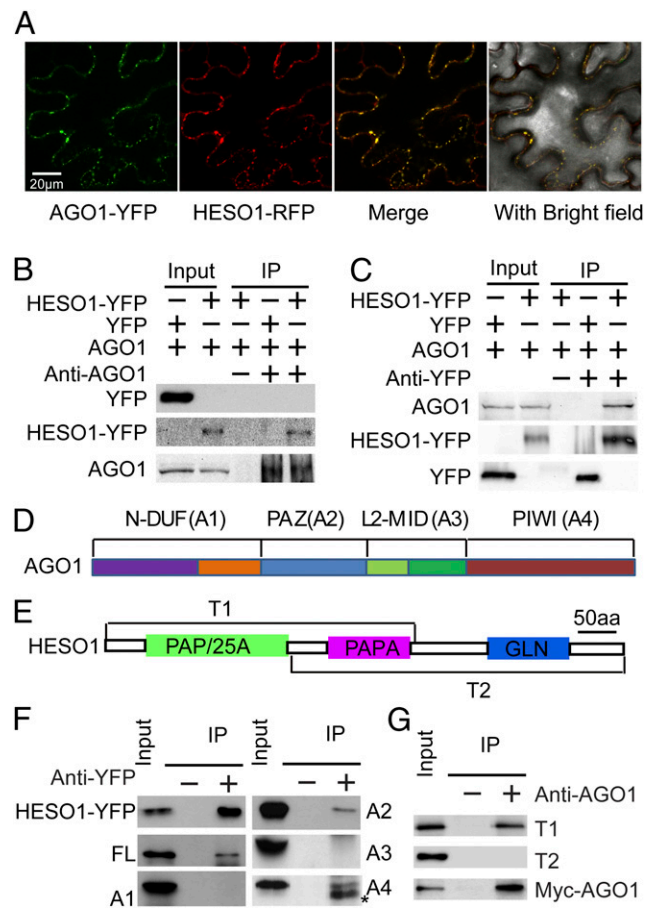
Fig. 4. HESO1 interacts with AGO1. (*A*) Colocalization of HESO1-RFP and AGO1-YFP. HESO1-RFP and AGO1-YFP fusion proteins were coinfiltrated into *N. benthamiana* leaves, and RFP and YFP fluorescence signals were monitored 48 h after infiltration by confocal microscopy. (*B*) HESO1-YFP coimmunoprecipitates with AGO1. (*C*) AGO1 co-IPs with HESO1-YFP. The protein mixtures containing AGO1/HESO1-YFP or AGO1/YFP were incubated with anti-AGO1-protein A-agarose beads and anti-YFP-protein A-agarose beads to capture AGO1, HESO1-YFP, and YFP, respectively. (*D*) A schematic diagram of AGO1 domains and truncated AGO1 fragments used for coimmunoprecipitation assays. (*E*) A diagram of truncated HESO1 fragments used for coimmunoprecipitation assays. (*F*) HESO1 co-IPs with the PAZ and PIWI domains of AGO1. Anti-YFP-protein A agarose beads were incubated with the protein extracts containing HESO1-YFP and full-length AGO1 or a truncated AGO1 fragment (indicated on the left or right side of the image) to capture the HESO1-YFP complex. Full-length AGO1 and truncated AGO1 fragments were fused with 10XMYC at their *N*-termini. Please note only one IP picture was shown for HESO1-YFP. (*G*) The N-terminal region of HESO1 interacts with AGO1. Both IP and co-IP signals were detected by Western blot analyses; ∼10% (vol/vol) input (for detecting IP signals) and ∼1% input (for detecting co-IP signals) were analyzed in parallel.

∼63 kDa), and a C-terminal fragment that contains the PAP-associated domain and the glutamine-rich region (aa 200–511; T2; ∼62 kDa), were fused with YFP at their C terminus, expressed in *N. benthamiana*, and analyzed for interactions with AGO1. The results showed that T1, but not T2, interacted with AGO1 (Fig. 4G).

HESO1 Acts on AGO1-Bound miRNAs. The AGO1–HESO1 interaction suggested that HESO1 might act on miRNA in the AGO1 complex. If so, uridylation of miRNAs may require a functional AGO1. To test this, we crossed *ago1-27* carrying a point mutation in the PIWI domain of AGO1 into the null *hen1-1* mutant and examined the status of 3′ tailing of miRNAs in *ago1-27 hen1-1*. Northern blotting revealed that the tailing of miR159/319
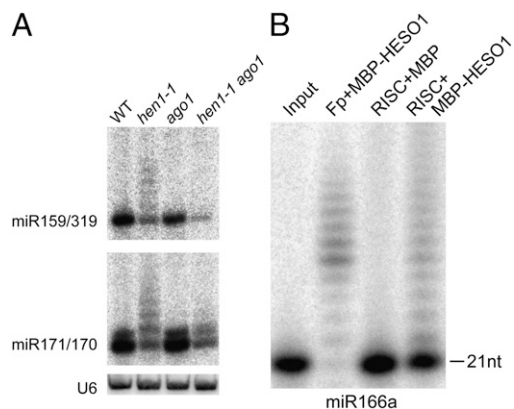
Fig. 5. HESO1 is able to uridylate an AGO1-bound miRNA in vitro. (A) The uridylation of miR159/319 and miR171/170 was reduced in ago1-27 hen1-1. (B) HESO1 lengthens AGO1-bound miR166a. The AGO1-miR166a complex or miR166a alone was incubated with HESO1-MBP or MBP in a reaction buffer containing UTP for 30 min. After the reactions, miR166a was extracted and separated by denaturing PAGE. MiR166a was [^{32}P] labeled at the 5′ end, using T4 Polynucleotide Kinase. Fp, Free probe.

and miR171/170 was dramatically impaired in *ago1-27 hen1-1* compared with *hen1-1* (Fig. 5A). Consistent with this result, the *ago1-11* mutation also reduces the tailing of many miRNAs in *hen1-2* (32). These results supported that HESO1 may uridylate miRNAs after AGO1 loading. We therefore examined whether HESO1 could act on AGO1-bound miRNA in vitro. We transiently expressed AGO1-YFP in *N. benthamiana* and immunoprecipitated the AGO1 complex using anti-AGO1 antibodies conjugated to protein A-agarose beads (Fig. S5A). The resulting AGO1 complex was incubated with 5′ [^{32}P]-labeled miR166a (unmethylated) to assemble the AGO1–miR166a complex, and unbound miR166a was removed through washing. AGO1–miR166a (Fig. S5B) was subsequently incubated with maltose-binding protein (MBP)-HESO1 or MBP in the presence of UTP. After washing, miR166a was extracted from the AGO1 complex and separated in a denaturing PAGE gel. miR166a was lengthened by MBP-HESO1, but not MBP, indicating that HESO1 is able to target AGO1-bound miRNA in vitro (Fig. 5B). It should be noted that endogenous *N. benthamiana* HESO1 might be coimmunoprecipitated with AGO1 as well. However, its amount might be too low to contribute to the lengthening of AGO1-bound miR166a in our assay, as no obvious activity was detected in the control reaction (Fig. 5B).

Discussion

In this study, we show that HESO1, a miRNA nucleotidyl transferase, uridylates 5′ fragments produced by miRNA-mediated target cleavage. We also reveal that HESO1 associates with AGO1 and acts on AGO1-bound miRNAs in vitro. Because both miRNAs and 5′ fragments are associated with AGO1 during the cleavage process, we propose that HESO1 can uridylate its substrates in the AGO1 complex (Fig. 6). However, the 3′ end of a miRNA may be protected by the PAZ domain of AGO1, which may reduce its exposure to HESO1. It is tempting to speculate that the uridylation of unmethylated miRNAs by HESO1 may depend on base-pairing between miRNAs and their targets in vivo, as base-pairing with targets is predicted to release the 3′ end of miRNAs from the PAZ domain (33). Consistent with this notion, miRNA uridylation is blocked when AGO1 function is impaired in *hen1* (Fig. 5A) (32), and extensive complementarity between targets and miRNAs triggers miRNA tailing in animals (34). However, the majority of miRNAs are normally methylated in plants, which prevents HESO1 function and, therefore, maintains the recycling of the miRNA–AGO1 complex (15, 20, 21, 35). Lack of HESO1 cannot completely eliminate uridylated 5′ fragments and miRNAs (20, 21), indicating that one or more HESO1

homologs may function redundantly with HESO1 in the miRNA pathway.

The abundance of 5′ fragments is increased in *heso1-2* relative to L*er*, demonstrating that uridylation induces the degradation of 5′ fragments (Figs. 2B and 6B). How does uridylation trigger 5′ fragment degradation? In *Drosophila* and *C. reinhardtii*, it has been observed that 5′ fragments can be degraded through 3′-to-5′ exonuclease activities (8, 27). However, the relative levels of 5′ fragments with 3′ truncation in both capped and uncapped 5′ fragment populations in *heso1-2* are increased compared with those in L*er*, suggesting that uridylation may trigger activities other than 3′-to-5′ exonucleases in *Arabidopsis* (Figs. 3 and 6). In fact, oligouridylation could prevent RNA from 3′ to 5′ degradation in vitro (36). However, we cannot rule out the possibility that 3′-to-5′ degradation activities triggered by uridylation are highly progressive, such that no or few 3′ truncation intermediates are accumulated in vivo. In both *heso1* and L*er*, 5′ fragments with 5′ truncation exist, suggesting that 5′-to-3′ degradation of 5′ fragments may occur. Indeed, XRN4 can degrade the 5′ fragments. However, it is possible that the 5′-to-3′ truncation of 5′ fragment occurs independent of uridylation, as lack of uridylation has no obvious effect on 5′-to-3′ truncation of 5′ fragments. The presence of capped and uncapped *MYB33-5′* with 3′ truncation indicates that they both can be degraded through 3′-to-5′ degradation activities (Fig. 3), which may be a slow process, and compete with HESO1 for substrates in *Arabidopsis* (Fig. 3). The enzymes degrading 5′ fragments from 3′-to-5′ remain to be identified, as the abundance of MYB33-5′ is not altered in exosome mutants *rrp6l1 rrp6l2 rrp6l3* and *csl4* (Fig. S3). In humans and yeast, uridylation has been shown to induce decapping of some RNAs, followed by degradation (36–38). The ratio of uridylated *MYB33-5′* in the uncapped population is higher than that in the capped population in L*er*, suggesting that uridylation may also have a role in stimulating decapping. Clearly, this possibility needs to be examined in the near future.
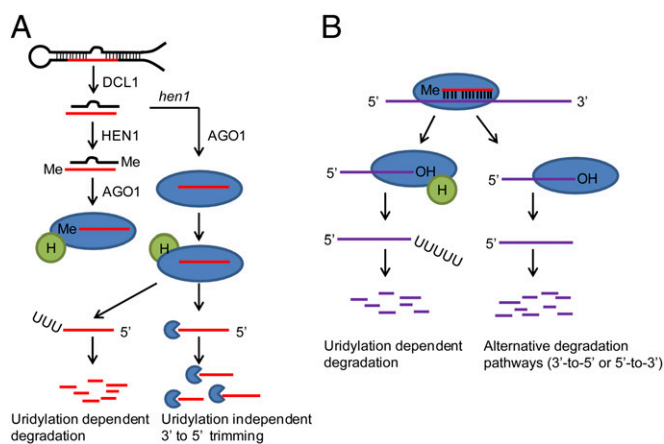
Materials and Methods

Fig. 6. A proposed model for HESO1 function in *Arabidopsis*. (A) HESO1 uridylates unmethylated miRNAs to lead to its degradation. (B) HESO1 uridylates the 5′ fragment to promote its degradation. Both 3′-to-5′ trimming activities and HESO1 target 5′ fragments and unmethylated miRNAs. HESO1-mediated uridylation triggers the degradation of 5′ fragments through a mechanism that is likely different from 3′-to-5′ trimming activities. Me, 3′ methyl group; H, HESO1; blue oval, AGO1.

GENETICS

Plasmid. HESO1 and AGO1 CDS were amplified by RT-PCR and cloned into Gateway vector pB7WGR2,0 (39) and pEarleyGate 101 (40) to generate HESO1-RFP and AGO1-YFP-HA, respectively. To express truncated AGO1 and HESO1, different AGO1 fragments (A1–A4) and HESO1 fragments (T1 and T2) were PCR-amplified and cloned into the Gateway vectors pGWB521 (41) and pEarleyGate101 to generate YFP (YFP fused at C terminus)-tagged and 10XMYC (10XMYC fused at N terminus)-tagged proteins, respectively. Primer sequences are listed in Table S1.

Protein Expression, Confocal Microscopy, Protein Size Fractionation, and Coimmunoprecipitation. Protein expression in *N. benthamiana* and *Escherichia coli* strain BL21, confocal microscopy, and coimmunoprecipitation were performed as described (42). The affinity-purified anti-AGO1 antibodies recognizing the N-terminal peptide of AGO1 (*N*-MVR KRRTDAPSC-C; ref. 6) were produced by GenScript. Anti-GFP (Clontech) and anti-AGO1 were precoupled to protein A agarose beads (Santa Cruz) and used for IP analyses. Anti-GFP, anti-MYC, and anti-AGO1 antibodies were used for Western blot detection of the respective proteins.

AGO1-miR166a Assembly and Terminal Uridyl Transferase Assay. The AGO1-miR166a complex was prepared according to ref. 5 and used for an in vitro terminal uridyl transferase assay (20). The detailed protocol can be found in *SI Materials and Methods*.

Al-RACE and cRACE. Al-RACE and cRACE were performed according to ref. 9, with some modifications. In the al-RACE experiment, 5 μg total RNA was first ligated to 100 pmol RNA adaptor by T₄ RNA ligase. In the cRACE experiment, 5 μg treated (CIP followed by TAP) or nontreated RNAs were subjected to self-ligation. First-strand cDNA was synthesized using the 3′ RT primer (for al-RACE) or the R1 primer (for cRACE). First-round PCR was performed using 3′RT/F1 (for al-RACE) or R1/F1 (for cRACE), and then 1 μL PCR product was diluted 50 times and used for the second round of PCR, using 3′RT/F2 (For al-race) or R2/F2 (for cRACE) and F2. The PCR products were cloned into pGEM-T Easy Vector (Promega) and sequenced. Primer sequences are listed in Table S1.

Northern Blot. Small RNA Northern blot was conducted as described (43). To detect *MYB33-5′* or *MYB33- 3′* by Northern blot, 30 μg total RNAs were resolved by electrophoresis on a 1.2% denaturing-formaldehyde agarose gel and transferred onto Zeta-probe membranes (Bio-Rad). Membranes were UV cross-linked and hybridized with probes recognizing *MYB33-5′* or *MYB33-3′*. Radioactive signals were detected using a Typhoon 9500 phosphorimager.

1. Chen XM (2009) Small RNAs and their roles in plant development. *Annu Rev Cell Dev Biol* 25:21–44.
2. Kim VN, Han J, Siomi MC (2009) Biogenesis of small RNAs in animals. *Nat Rev Mol Cell Biol* 10(2):126–139.
3. Hutvagner G, Simard MJ (2008) Argonaute proteins: Key players in RNA silencing. *Nat Rev Mol Cell Biol* 9(1):22–32.
4. Schwab R, et al. (2005) Specific effects of microRNAs on the plant transcriptome. *Dev Cell* 8(4):517–527.
5. Baumberger N, Baulcombe DC (2005) Arabidopsis ARGONAUTE1 is an RNA Slicer that selectively recruits microRNAs and short interfering RNAs. *Proc Natl Acad Sci USA* 102(33):11928–11933.
6. Qi Y, Denli AM, Hannon GJ (2005) Biochemical specialization within Arabidopsis RNA silencing pathways. *Mol Cell* 19(3):421–428.
7. Vaucheret H, Vazquez F, Crété P, Bartel DP (2004) The action of ARGONAUTE1 in the miRNA pathway and its regulation by the miRNA pathway are crucial for plant development. *Genes Dev* 18(10):1187–1197.
8. Orban TI, Izaurralde E (2005) Decay of mRNAs targeted by RISC requires XRN1, the Ski complex, and the exosome. *RNA* 11(4):459–469.
9. Shen BZ, Goodman HM (2004) Uridine addition after microRNA-directed cleavage. *Science* 306(5698):997.
10. Hagan JP, Piskounova E, Gregory RI (2009) Lin28 recruits the TUTase Zcchc11 to inhibit let-7 maturation in mouse embryonic stem cells. *Nat Struct Mol Biol* 16(10):1021–1025.
11. Heo I, et al. (2009) TUT4 in concert with Lin28 suppresses microRNA biogenesis through pre-microRNA uridylation. *Cell* 138(4):696–708.
12. Heo I, et al. (2012) Mono-uridylation of pre-microRNA as a key step in the biogenesis of group II let-7 microRNAs. *Cell* 151(3):521–532.
13. Newman MA, Mani V, Hammond SM (2011) Deep sequencing of microRNA precursors reveals extensive 3′ end modification. *RNA* 17(10):1795–1803.
14. Ameres SL, Hung JH, Xu J, Weng ZP, Zamore PD (2011) Target RNA-directed tailing and trimming purifies the sorting of endo-siRNAs between the two Drosophila Argonaute proteins. *RNA* 17(1):54–63.
15. Li JJ, Yang ZY, Yu B, Liu J, Chen XM (2005) Methylation protects miRNAs and siRNAs from a 3′-end uridylation activity in Arabidopsis. *Curr Biol* 15(16):1501–1507.
16. Kamminga LM, et al. (2010) Hen1 is required for oocyte development and piRNA stability in zebrafish. *EMBO J* 29(21):3688–3700.
17. Jones MR, et al. (2009) Zcchc11-dependent uridylation of microRNA directs cytokine expression. *Nat Cell Biol* 11(9):1157–1163.
18. van Wolfswinkel JC, et al. (2009) CDE-1 affects chromosome segregation through uridylation of CSR-1-bound siRNAs. *Cell* 139(1):135–148.
19. Ibrahim F, et al. (2010) Uridylation of mature miRNAs and siRNAs by the MUT68 nucleotidyltransferase promotes their degradation in Chlamydomonas. *Proc Natl Acad Sci USA* 107(8):3906–3911.
20. Ren GD, Chen XM, Yu B (2012) Uridylation of miRNAs by hen1 suppressor1 in Arabidopsis. *Curr Biol* 22(8):695–700.
21. Zhao YY, et al. (2012) The Arabidopsis nucleotidyl transferase HESO1 uridylates unmethylated small RNAs to trigger their degradation. *Curr Biol* 22(8):689–694.
22. Wyman SK, et al. (2011) Post-transcriptional generation of miRNA variants by multiple nucleotidyl transferases contributes to miRNA transcriptome complexity. *Genome Res* 21(9):1450–1461.
23. Rhoades MW, et al. (2002) Prediction of plant microRNA targets. *Cell* 110(4):513–520.
24. Mallory AC, Bartel DP, Bartel B (2005) MicroRNA-directed regulation of Arabidopsis AUXIN RESPONSE FACTOR17 is essential for proper development and modulates expression of early auxin response genes. *Plant Cell* 17(5):1360–1375.
25. Llave C, Xie ZX, Kasschau KD, Carrington JC (2002) Cleavage of Scarecrow-like mRNA targets directed by a class of Arabidopsis miRNA. *Science* 297(5589):2053–2056.
26. Millar AA, Gubler F (2005) The Arabidopsis GAMYB-like genes, MYB33 and MYB65, are microRNA-regulated genes that redundantly facilitate anther development. *Plant Cell* 17(3):705–721.
27. Ibrahim F, Rohr J, Jeong WJ, Hesson J, Cerutti H (2006) Untemplated oligoadenylation promotes degradation of RISC-cleaved transcripts. *Science* 314(5807):1893.
28. Kastenmayer JP, Green PJ (2000) Novel features of the XRN-family in Arabidopsis: Evidence that AtXRN4, one of several orthologs of nuclear Xrn2p/Rat1p, functions in the cytoplasm. *Proc Natl Acad Sci USA* 97(25):13985–13990.
29. Souret FF, Kastenmayer JP, Green PJ (2004) AtXRN4 degrades mRNA in Arabidopsis and its substrates include selected miRNA targets. *Mol Cell* 15(2):173–183.
30. Zhao YY, Mo BX, Chen XM (2012) Mechanisms that impact microRNA stability in plants. *RNA Biol* 9(10):1218–1223.
31. Xie M, Ren GD, Costa-Nunes P, Pontes O, Yu B (2012) A subgroup of SGS3-like proteins act redundantly in RNA-directed DNA methylation. *Nucleic Acids Res* 40(10):4422–4431.
32. Zhai JX, et al. (2013) Plant microRNAs display differential 3′ truncation and tailing modifications that are ARGONAUTE1 dependent and conserved across species. *Plant Cell* 25(7):2417–2428.
33. Yuan YR, et al. (2005) Crystal structure of A. aeolicus argonaute, a site-specific DNA-guided endoribonuclease, provides insights into RISC-mediated mRNA cleavage. *Mol Cell* 19(3):405–419.
34. Ameres SL, et al. (2010) Target RNA-directed trimming and tailing of small silencing RNAs. *Science* 328(5985):1534–1539.
35. Yu B, et al. (2005) Methylation as a crucial step in plant microRNA biogenesis. *Science* 307(5711):932–935.
36. Song MG, Kiledjian M (2007) 3′ Terminal oligo U-tract-mediated stimulation of decapping. *RNA* 13(12):2356–2365.
37. Mullen TE, Marzluff WF (2008) Degradation of histone mRNA requires oligouridylation followed by decapping and simultaneous degradation of the mRNA both 5′ to 3′ and 3′ to 5′. *Genes Dev* 22(1):50–65.
38. Rissland OS, Norbury CJ (2009) Decapping is preceded by 3′ uridylation in a novel pathway of bulk mRNA turnover. *Nat Struct Mol Biol* 16(6):616–623.
39. Karimi M, Inzé D, Depicker A (2002) GATEWAY vectors for Agrobacterium-mediated plant transformation. *Trends Plant Sci* 7(5):193–195.
40. Earley KW, et al. (2006) Gateway-compatible vectors for plant functional genomics and proteomics. *Plant J* 45(4):616–629.
41. Tanaka Y, Nakamura S, Kawamukai M, Koizumi N, Nakagawa T (2011) Development of a series of gateway binary vectors possessing a tunicamycin resistance gene as a marker for the transformation of Arabidopsis thaliana. *Biosci Biotechnol Biochem* 75(4):804–807.
42. Ren GD, et al. (2012) Regulation of miRNA abundance by RNA binding protein TOUGH in Arabidopsis. *Proc Natl Acad Sci USA* 109(31):12817–12821.
43. Park W, Li JJ, Song RT, Messing J, Chen XM (2002) CARPEL FACTORY, a Dicer homolog, and HEN1, a novel protein, act in microRNA metabolism in Arabidopsis thaliana. *Curr Biol* 12(17):1484–1495.

Supporting Information

Ren et al. 10.1073/pnas.1405083111

SI Materials and Methods

Argonaute–miR166a Assembly and Terminal Uridyl Transferase Assay.
To test HUA1 enhancer 1 (HEN1) suppressor 1 (HESO1) activity on long single-stranded RNA (ssRNA), a portion of *UBQ5* CDS was PCR amplified and used as a template to synthesize ssRNA, using T7 RNA polymerase in the presence of [α-^{32}P] UTP. Fifty nanograms maltose-binding protein (MBP) or MBP-HESO1 were incubated with [^{32}P]-labeled RNA in the New England Biolabs 2 buffer with 40 U RNase inhibitor and 1 mM UTP at 25 °C. The reaction was stopped by the addition of the formamide/EDTA RNA sampling buffer.

To assemble the Argonaute (AGO1)–miR166a complex, proteins from *N. benthamiana* leaves expressing AGO1 fused with a yellow fluorescence protein (AGO1-YFP) were extracted using extraction buffer (50 mM Tris·Cl at pH 7.5, 150 mM NaCl, 5 mM MgCl2, 5% glycerol, 2mM DTT, 0.1mM PMSF, and 1/100 protease inhibitor). The AGO1-YFP complex was immuno-precipitated overnight at 4 °C with anti-AGO1 coupled to pro-tein A-agarose beads. The AGO1-YFP complex were incubated with [^{32}P]-labeled miR166a (unmethylated) in 0.5 mL protein extraction buffer containing 20 U RNase inhibitor for 1 h and then washed three times with protein extraction buffer. The AGO1–miR166a complex was then subjected to the terminal uridyl transferase assay in the presence of 1 mM ATP and 1 mM UTP. The beads were washed three times after 30 min in-cubation, and AGO1-bound miR166a was extracted and ana-lyzed on a 16% polyacrylamide denaturing gel. The radioactive signals were detected using a Typhoon 9500 phosphorimager.
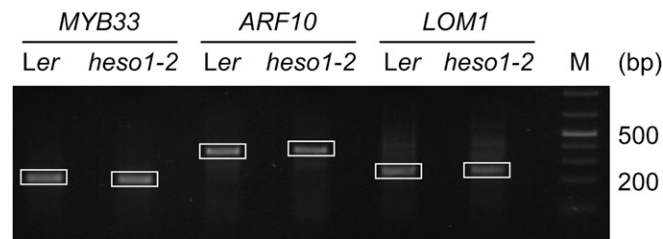
Fig. S1. Adaptor-ligation mediated rapid amplification of cDNA ends (al-RACE) cloning of 5′ fragments. Total RNAs from Landsberg *erecta* (L*er*) or *heso1-2* were ligated to a 3′ RNA adaptor and subjected to 3′ al-RACE, which was followed by RT-PCR. The nested-PCR products were resolved in a 1.5% (vol/vol) agarose gel. DNAs of the expected size were gel purified before cloning (white boxes).
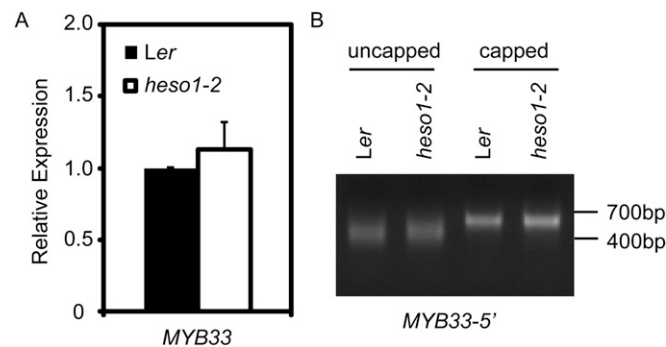

Fig. S2. Circularized rapid amplification of cDNA ends (cRACE) cloning of the capped and uncapped 5′ fragment of *MYB domain protein 33* (*MYB33-5′*). (*A*) Quantitative RT-PCR analysis of *MYB33* transcripts using primers that span the microRNA cleavage site. (*B*) RT-PCR analysis of cRACE products of uncapped and capped *MYB33-5′* in L*er* and *heso1-2*. Total RNAs with or without the sequential treatment by alkaline phosphatase, calf intestinal, and tobacco acid py-rophosphatase were subjected to self-ligation (see Fig. 2 *A* and *B*). The nested-PCR products were resolved in a 1.5% (vol/vol) agarose gel.
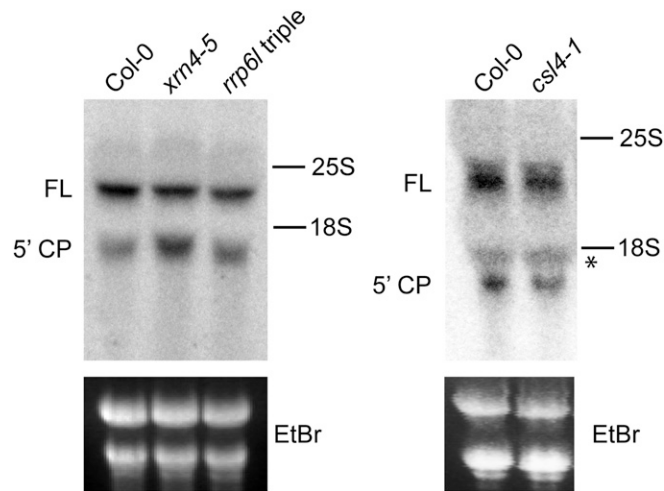
Fig. S3. The accumulation of *MYB33-5′* is increased in *exoribonuclease 4-5* (*xrn4-5*). *MYB33* RNAs in wild-type control, *xrn4-5*, *rrp6l1 rrp6l2 rrp6l3* (*rrp6l* triple), and *csl4-1* were detected by Northern blotting, using the 5′ probe shown in Fig. 2A. FL, full-length *MYB33* transcripts; 5′ CP, 5′ cleavage product. *Nonspecific signal.
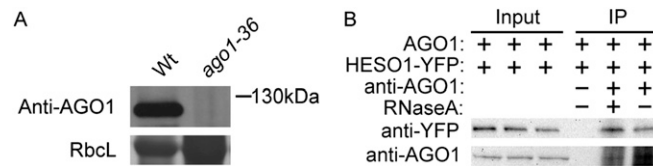

Fig. S4. HESO1 interacts with AGO1 in an RNA-independent manner. (*A*) Examination of anti-AGO1 antibodies by Western blot. The *ago1-36* mutant, a null allele of *ago1*, was used as a negative control. A 1:2,000 (vol/vol) dilution of anti-AGO1 was used for the Western blot. Larger-chain gene of ribulose-1,5-bisphosphate carboxylase (RbcL) was visualized by staining with Coomassie brilliant blue. (*B*) The HESO1–AGO1 interaction is resistant to the RNase A treatment.
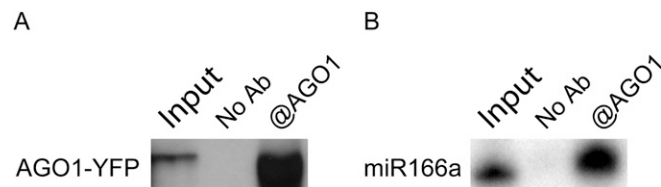

Fig. S5. Assembling of the AGO1–miR166a complex in vitro. (*A*) Immunoprecipitation of AGO1-YFP by anti-AGO1 coupled with protein A beads. Proteins were resolved on an SDS-polyacrylamide gel and detected by Western blot with an anti-YFP antibody (Covance). (*B*) Detection of [^{32}P]-labeled miR166a in the AGO1 complex.

Table S1. Primers used in this study

Name	Sequence (5′ – 3′)	Applications
Plasmid construction		
HESO1gGWF	CACCATTCTCTCATGTGGAACGAG	*pHESO1*-HESO1-YFP
HESO1gGWR	CTGCTCATGTCTCGGTCTCCAGA	
HESO1cGWF	CACCATGAGTAGAAACCCTTTCCTG	HESO1-RFP
HESO1cGWR	CTGCTCATGTCTCGGTCTCCAGA	
HESO1-T1F	CACCATGAGTAGAAACCCTTTCCTGG	HESO1-T1
HESO1-T1R	TATTCTGTCCAAATTTCTACGG	
HESO1-T2F	CACCATGGCAATCTTGCCGCCTCTAAGAG	HESO1-T2
HESO1-T2R	CTGCTCATGTCTCGGTCTCCAG	
AGO1cGWF	CACCATGGTGAGAAAGAGAAGAACG	AGO1-YFP
AGO1cNS GWR	GCAGTAGAACATGACACGCTTCAC	
A1-GWF	CACCATGGTGAGAAAGAGAAGAACG	10XMYC-A1
A1-GWR	CTAAGGGTTTGCCTCTATGAAGGC	
A2-GWF	CACCTCATCGACAGCCTTCATAGAG	10XMYC-A2
A2-GWR	CTATCGATCTATCGGGCGCTGACA	
A3-GWF	CACCAAGGTTACCTGTCAGCGCCCGAT	10XMYC-A3
A3-GWR	CTAAGTCTCACATATGCGTTTCAA	
A4-GWF	CACCTCCCAAGGAAAAGAAATTGATC	10XMYC-A4
A4-GWR	TCAGCAGTAGAACATGACACGCTTC	
In vitro transcription		
T7-UBQ5F	taatacgactcactatagggATGCAGATCTTCGTGAAAACC	100 nt ssRNA
UBQ5 R2	GGATTCCTTCCTTGTCTTGGA	
Small RNA probes		
miR159/319	GGG+AGC+TCC+CTT+CAG+TCC+AA	Northern blot
U6	TCATCCTTGCGCAGGGGCCA	Northern blot
Primers for qRT-PCR		
MYB33qF	CTACGGATGGCATTGTTCCT	qRT-PCR
MYB33qR	GGTGGTGGTGGAGACTGAAT	
N_UBQ5	GGTGCTAAGAAGAGGAAGAAT	qRT-PCR, Southern blot probe
C_UBQ5	CTCCTTCTTTCTGGTAAACGT	
Al-RACE and cRACE		
RNA Adaptor	pUUUdCdTdGdTdAdGdGdCdAdCdCdAdTdCdAdAdTidT	For RNA ligation
3′RT	ATTGATGGTGCCTACAG	RT and PCR
MYB33F1	AAGCGACTTTGGGAATCTGA	MYB33 RACE-PCR
MYB33R1	GCCATACGTGCCCATCTATT	
MYB33F2	AAGAATTCTCGTCGCCTGAA	
MYB33R2	TTGGCCTCAGATGATTAGCC	
LOM1F1	TTATCTCCACCGGCTAAACG	LOM1 RACE-PCR
LOM1F2	TCGTCGTCAACATCAGTTTCA	
ARF10F1	GGACAAGCGTTTGAGGTTGT	ARF10 RACE-PCR
ARF10F2	AATGGCGTTTGAAACAGAGG	
Northern Blot		
MYB33 NpF	AAGCGACTTTGGGAATCTGA	MYB33 5′ probe
MYB33 NpR	AGGAACAATGCCATCCGTAG	
MYB33 CpF	CACCAAGGCAGAGAGAAAAAAGCG	MYB33 3′ Probe
MYB33 CpR	ACAGGTGGCATGTTGCTCCAAGAAC	

qRT-PCR, quantitative RT-PCR.

Other Supporting Information Files